Evaluation of ACI CODE 440.11-22 Design Provisions for GFRP-RC Columns: Constitutive Models and Practical Interaction Diagrams

Alireza Sadat Hosseini* and Pedram Sadeghian
Department of Civil and Resource Engineering, Dalhousie University, Halifax, NS, Canada
*Corresponding author – email: asadat@dal.ca

ABSTRACT

With the release of ACI CODE-440.11-22, which introduces design provisions for GFRP-Reinforced Concrete (RC) columns, it is important to evaluate the limitations of the adopted approach and provide practical design tools. This study develops and validates an analytical cross-sectional model—based on equilibrium and strain compatibility—against theoretical and experimental data, to generate axial load–bending moment (N–M) interaction diagrams for short GFRP-RC columns in accordance with the new code. The model uses the equivalent rectangular stress block for concrete in compression and incorporates key design parameters, including GFRP bar properties and strength reduction factors. To assess the conservatism of the code approach, the study compares interaction diagrams generated using the code's stress block with those developed using nonlinear concrete constitutive models. Results show that the code-based diagrams are more conservative, and a scaling factor of 1.1 is suggested to better match actual behavior. As the ACI code neglects the compressive contribution of GFRP bars, their tensile strength affects only the tension side of the interaction diagram. Moreover, variations in the bar's elastic modulus influence the diagram from the balance point on the tension side up to the point where all bars are in compression and thus excluded from the analysis.

DOI: https://doi.org/10.1002/suco.70209

Keywords: Concrete Column; GFRP Bar; Load Eccentricity; Interaction Diagram; Concrete Constitutive Model

1. INTRODUCTION

Due to extensive research on Glass Fiber Reinforced Polymer (GFRP)-Reinforced Concrete (RC) columns, including GFRP bars' contribution to load bearing in concentrically loaded columns (1–17), eccentricity effects (6,7,9,11,15,18–27), and transverse reinforcement (1,2,5,6,9,11–14,20,22,28–35) ACI CODE-440.11-22 (36) allocated a chapter to the design of GFRP-RC columns which was not in the ACI 440.1R-15 guideline before (37). Also, the Canadian Highway Bridge Design Code, CSA S6-19 (38) no longer neglects the contribution of GFRP bars in compression, and a contribution to a load bearing of up to a stress level corresponding to a strain of 0.002 in bars is considered. ACI CODE-440.11-22 (36) allows short column analysis (neglecting the slenderness effects) when slenderness ratio, which is the ratio of the effective length of the column to its least radius of gyration (kl_u/r), is less than or equal to 17 for columns which are not braced against sideways, and for braced frames it is a function of end moments ratio. Previous studies have investigated slenderness limits using theoretical models (39), experimental and analytical studies (40), axial load capacity reduction (41), force ratio (42), with proposed limits typically ranging from 14 to 18.

The code considers design limits for the dimensions of the column and limits the tensile strain of the longitudinal bars to 0.01. Also, there are strength limits and new criteria are imposed for strength reduction factor based on the strain of the longitudinal reinforcement for columns under axial load and bending moment. For the design, equivalent rectangular stress block is assumed for concrete wherein the concrete stress is 0.85 of the concrete strength, f'_c, and the depth of block is $\beta_1 C_{NA}$ (C_{NA} is the neutral axis depth). For calculating β_1, a table is provided based on the concrete compressive strength ranges.

RC columns are subjected to combined axial loads and bending moments due to factors like construction imperfections and architectural requirements. Column interaction diagrams are used to evaluate their axial and flexural resistance, with load eccentricity significantly influencing behavior. GFRP-reinforced columns have been studied experimentally, analytically, and numerically under concentric and eccentric loads. Given the inevitable occurrence of eccentricity in axial loads, the impact of eccentricity on GFRP-reinforced concrete columns is a topic of discussion. Some researchers argue for disregarding the contribution of FRP bars under eccentric loading (9,18,19), whereas others contend that it should not be overlooked (6,20–22).

Khorramian and Sadeghian (7) tested GFRP-RC columns subjected to both concentric and eccentric compressive loads. The results showed that GFRP bars did not crush at column peak load and sustained high strains without reaching their compressive strain capacity and should not be ignored. Full-scale GFRP-RC columns with different longitudinal reinforcement ratios and under various levels of eccentricity were tested by Guérin et al. (22). The effect of the reinforcement ratio on strength, failure mode, deformation, and strain behavior of the columns was studied, and experimental axial force-moment (P-M) interaction diagrams were created for each group. It was shown that including GFRP bars' compression contribution improved P-M diagram accuracy, while neglecting it increased conservativeness. In another study by Guérin et al. (31), square GFRP-RC columns with GFRP ties tested under different levels of eccentricity. The GFRP-RC columns exhibited similar behavior to steel-RC columns, with eccentricity significantly impacting strength and failure modes. Sun et al. (21) investigated the behavior of GFRP-RC columns subjected to three initial eccentricities. Results showed that columns experienced concrete crushing on the pressure side, but the GFRP bars mostly remained intact. It was also found that bond behavior between the GFRP bars and concrete improved when the GFRP bars were used as

longitudinal compressive bars. Hadhood et al. (3), (4) investigations on full-scale circular GFRP-RC columns showed that failure modes vary with eccentricity, from compression-controlled for concentric loading to primary flexural-tension for high eccentricity. Elchalakani and Ma (9) tested rectangular concrete columns reinforced with steel and GFRP bars to failure under various loading conditions, examining the effect of load eccentricity, ligature spacing, and confinement area on axial capacity and ductility. Results showed that GFRP-RC columns with less concrete cover achieved greater strain and deformation ductility than equivalent steel-reinforced columns. Testing GFRP-RC columns by Hadi et al. (18) indicated that steel-reinforced specimens outperform those with GFRP bars in load capacity and ductility, with a 4.8% lower load capacity for concentric loading and an average 18.5% lower capacity for eccentric loading.

Elmesalami et al. (16) tested concrete columns reinforced with FRP bars under both concentric and eccentric loading. The results showed that columns reinforced with basalt-FRP (BFRP) and GFRP had similar load-carrying capacity, which was lower than that of steel-reinforced columns. The contribution of FRP bars to the ultimate capacity was approximately 11% for both GFRP and BFRP, compared to 31% for steel bars. Circular RC columns were tested under concentric axial load and were reinforced with longitudinal GFRP and CFRP bars, while being confined with circular FRP spirals or hoops (11). The results showed that the GFRP and CFRP bars were effective in resisting compression until after crushing of concrete. In a study by Salah-Eldin et al. (43), full-scale concrete columns with varying eccentricity-to-width ratios, concrete strength, and reinforcement types (steel and GFRP bars and ties) were tested under axial monotonic loading. Despite the different conditions, the test results showed that the failure of the specimens was not caused by GFRP bar rupture on the tension side, but rather by the maximum section capacity limit imposed by concrete strain. Khorramian and Sadeghian (25) tested large-scale concrete columns

reinforced with GFRP bars with different slenderness ratios and reinforcement ratios under eccentric compression. Results showed that the GFRP bars sustained load and moment after concrete spalling until compression failure, demonstrating their contribution. More recently, Wang et al. (44) found that columns with integrated steel spirals, those having outer GFRP bars showed 3 to 10 % lower peak loads than those with steel bars. In another study, the effect of transverse reinforcement with a new test procedure was investigated (45). Nouri et al. (46) implemented machine learning approach for predicting the axial capacity of GFRP columns. ACI CODE-440.11-22 does not include seismic provisions, primarily due to the lack of a proven methodology to ensure adequate ductility and energy dissipation in GFRP-RC members. However, recent studies have investigated the seismic performance of GFRP-RC columns (47), systems with internal (48) and external (49) GFRP tubes, hybrid reinforcement (47), highlighting the need for continued research and future code development in this area.

As reviewed, numerous experimental, numerical, and analytical studies have been conducted to investigate the behavior of GFRP-RC columns under combined axial and bending moments, leading to the development of interaction diagrams. While previous studies have explored the contribution of GFRP bars and produced interaction diagrams, the recent release of ACI CODE-440.11-22 (36), which includes a dedicated chapter (Chapter 10) on column design, emphasizes the need for updated interaction diagrams that align with the new code requirements and address its limitations for practical design applications. This paper presents interaction diagrams for rectangular and circular cross-section columns reinforced with GFRP bars, considering a practical range of material properties and dimensional characteristics. The novelty of the study lies in its systematic application of ACI CODE-440.11-22 (36) clauses, marking the first effort to generate interaction diagrams strictly based on the new code's provisions. Prior to preparing the interaction

diagrams, the relevant code clauses are thoroughly discussed to ensure accurate interpretation and alignment with the code's intent. In addition, the study evaluates the conservativeness of the ACI approach for stress distribution in concrete by comparing it with nonlinear concrete constitutive models. A parametric study is also conducted to assess the influence of GFRP material properties, such as ultimate tensile strength and elastic modulus, on the interaction diagrams. By addressing both the conservativeness of the code and the impact of GFRP material properties, the paper contributes valuable insights for both researchers and practitioners, helping bridge the gap between theoretical provisions and real-world applications.

3. ANALYTICAL MODEL

The study's analytical model utilizes cross-sectional analysis to determine the stress and strain of FRP bars and concrete for different combinations of axial compressive loads and corresponding moments due to load eccentricity. The column's cross-section comprises of n layers of GFRP bars, where each layer has an area of A_{fi} and a distance of d_i from the bottom of the section. GFRP bars are assumed to exhibit linear-elastic behavior until their ultimate strength, which is defined by the elastic modulus of the bar.

For the behavior of concrete, three approaches were considered. First, the conventional approach of design is used to prepare the design interaction diagrams. In this approach an equivalent stress block is considered for the concrete in compression while the contribution of concrete in tension is neglected. In the second and third approaches, two well-known constitutive models proposed by Popovics (50) and Thorenfeldt (51) are used and results are compared in the parametric studies section of the paper.

For any given value of the neutral axis depth, the strains in the GFRP bars are calculated based on the no-slip assumption between bars and concrete (i.e., surface roughness of GFRP bars provides

adequate bond with concrete). Therefore, a linear strain distribution exists in the cross section, and by considering the strain of the ultimate compressive layer of concrete, ε_{cm}, equal to 0.003 (clause R22.3.1.1) (36), the strain at each layer, ε_i, can be found using:

$$\varepsilon_i = \frac{\varepsilon_{cm}}{C_{NA}} y_i \quad (1)$$

The ultimate compressive strain of 0.003 is based on ACI CODE-440.11-22 (36), Clause R22.3.1.1, and reflects the same value adopted in ACI 318 (52) for concrete sections at ultimate conditions. This value is widely accepted in design codes because experimental tests have consistently shown that normal-strength concrete typically reaches failure at a compressive strain around 0.003 (53–56). In Eq. (1), C_{NA} is the depth of neutral axis, and y_i is the location of each layer in the section, measured from the top of the section height. Based on strain compatibility, Eq. (1) can be used to find the strain in bars based on their location, y_{fi}. Therefore, the strain in each bar can be calculated based on the location of the neutral axis. Having the strains in the bars, stress values are calculated using an elastic modulus, E_f, of 50 GPa for GFRP bars which is an average value in the practical range of manufactured GFRP bars. The ultimate tensile strength of GFRP bars, f_{fu}, is assumed to be 900 MPa, representing approximately the average minus one standard deviation based on available manufacturer data (Table 1).

Table 1. Strength values reported (in MPa) by different manufacturers of GFRP bars

	Bar size			
Manufacturer	#5 (15M)	#6 (20M)	#7 (22M)	#8 (25M)
A	1000	1000	1000	1000
B	970	900	880	840
C	1000	1000	1000	1000
D	1000	1000	1000	900
E	890	880	860	840
Mean values	972	956	948	916
Standard deviation	48	61	72	80

The mechanical properties of GFRP bars depend on several factors, including the type of fiber, typically E-glass, the fiber volume fraction, which is approximately 80% in modern bars, and the type of resin, most commonly vinyl ester due to its superior durability and chemical resistance. The average values reported in Table 1 represent the practical overall properties of the bars, determined using the standard test method for tensile properties of FRP bars (57). Previous research has demonstrated that while the compressive strength of GFRP bars is generally lower than their tensile strength due to mechanisms such as fiber micro-buckling and matrix crushing, but their elastic modulus in tension and compression is almost equal (58–62). However, according to ACI CODE-440.11-22 (36), the contribution of GFRP bars in compression is neglected. While this approach introduces conservatism, it contrasts with the Canadian Highway Bridge Design Code (CSA S6) (38), which permits the inclusion of GFRP bar compressive strength up to a strain of 0.002. In this study, the generation of interaction diagrams is based solely on the tensile properties of the GFRP bars to maintain full compatibility with the ACI code and to produce practical diagrams suitable for design applications.

An environmental reduction factor, $C_E = 0.85$, is applied to the average ultimate guaranteed tensile strength of the bars as per clause 20.2.2.3.

Concrete stress of $0.85f'_c$ is assumed uniformly distributed over an equivalent rectangular area with the stress block factor, β_1, which is considered as per clause 22.2.2.4.3 (36) ranging from 0.65 to 0.85 as a function of concrete compressive strength:

$$\beta_1 = \begin{cases} 0.85 & 20 \le f'_c \le 28 \\ 0.85 - 0.05\dfrac{(f'_c - 28)}{7} & 28 \le f'_c \le 55 \ (MPa) \\ 0.65 & 55 \le f'_c \end{cases} \quad (2)$$

According to Clause 21.2 of ACI CODE (36) the strength reduction factor, ϕ, for concrete under combined moment and axial force ranges from 0.55 to 0.65 based on the strain in the outermost

GFRP bar layer and the associated failure mode (Figure 1), with lower values applied to tension-controlled failures due to their sudden and brittle nature. This classification does not account for the influence of different transverse reinforcement types such as ties or spirals.

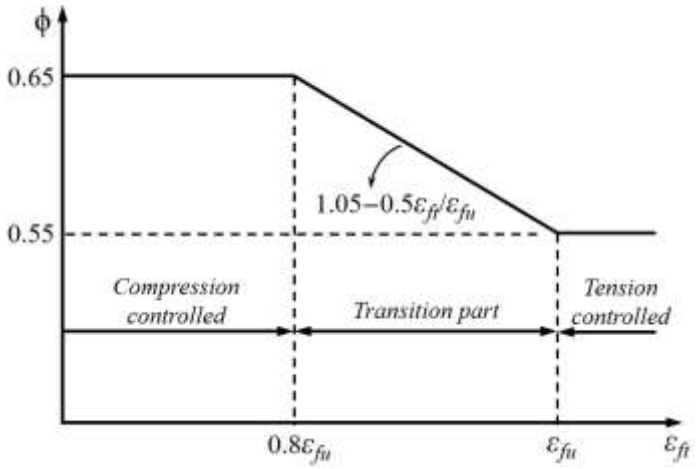

Figure 1. Strength reduction factor, ϕ, as a function of the net tensile strain in extreme tension reinforcement, ε_{ft}

The calculation of forces and moments in the concrete and reinforcement, based on the code requirements, is presented in the following subsections for rectangular and circular cross-section columns, respectively. The total force and moment in the concrete are calculated using the volume of the equivalent stress block, incorporating the reduction factor. For GFRP bars, forces and moments are determined as the sum of the forces and moments from each layer. The load eccentricity with respect to the center of plastic, e, is calculated by dividing the sum of the concrete and GFRP bar moments, M_T, by the sum of the forces, P_T:

$$e = \frac{M_T}{P_T} - C_{NA} + C_P \tag{3}$$

In which the ratio of M_T over P_T is the load eccentricity with respect to the neutral axis, and C_P is the depth of the plastic centroid of the section.

3.1. Rectangular Cross Section

Figure 2 shows the strain and stress distribution in the section. The compressive force is considered positive, and the moment is assumed to be applied around the neutral axis, C_{NA}.

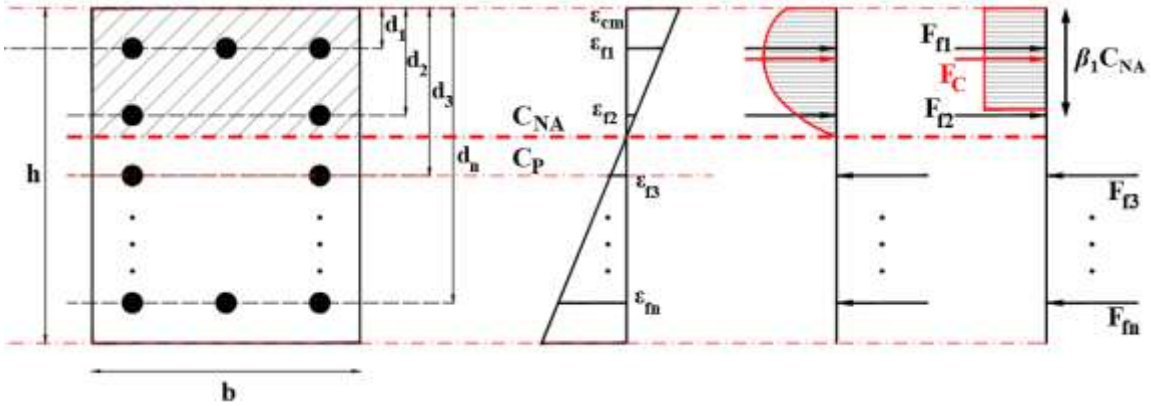

Figure 2. Parameters and assumptions for cross-sectional analysis of rectangular and circular column sections

For different values of the neutral axis, ranging from -∞ to +∞, the forces and moments in each layer of bars are calculated:

$$F_{fi} = f_{fi} \times A_{fi} \tag{4}$$

Wherein, f_{fi} is the stress at each layer of the FRP bar, calculated from the linear relationship between strain and stress using the GFRP elastic modulus, E_f. A_{fi} is the total area of the bars at the layer, and y_{fi} is the location of each bar layer. The moment around the neutral axis is calculated as:

$$M_{fi} = f_{fi} \times A_{fi} \times y_{fi} \tag{5}$$

Also, the moment with respect to the center of plastic can be calculated as:

$$M_{fi}{}' = f_{fi} \times A_{fi} \times y_{fi} \times (C_P - C_{NA}) \tag{6}$$

Then the force in the concrete is calculated (clause 22.2.2.4):

$$F_c = 0.85 f_c' \beta_1 C_{NA} b \tag{7}$$

Where b is the section width (Figure 2). And consequently, moments about neutral axis, M_c, and the center of plastic, M'_c, can be found by the following equations, respectively:

$$M_c = F_c(1 - 0.5\beta_1)C_{NA} \tag{8}$$

$$M_c{}' = F_c[(1 - 0.5\beta_1)C_{NA} + (C_P - C_{NA})] \tag{9}$$

The sum of concrete and GFRP bar forces gives the overall force, P_T, and moment, M_T, of the cross section for a certain location of the neutral axis, and therefore, load eccentricity can be calculated as described before. To account for accidental eccentricity, the nominal axial strength of the section in compression, P_n, is limited to $0.80P_0$ for columns with ties according to clause 22.4.2 (36) based on the work by Hadhood et al. (63) on circular ties. Where, P_0 is (clause 22.4.2.2):

$$P_0 = 0.85f_c'bh \tag{10}$$

3.2. Circular Cross Section

Similar to rectangular cross sections, for circular cross sections, the compressive force is considered to be positive, and the moment is assumed to be applied around the neutral axis, C_{NA} as per Figure 3.

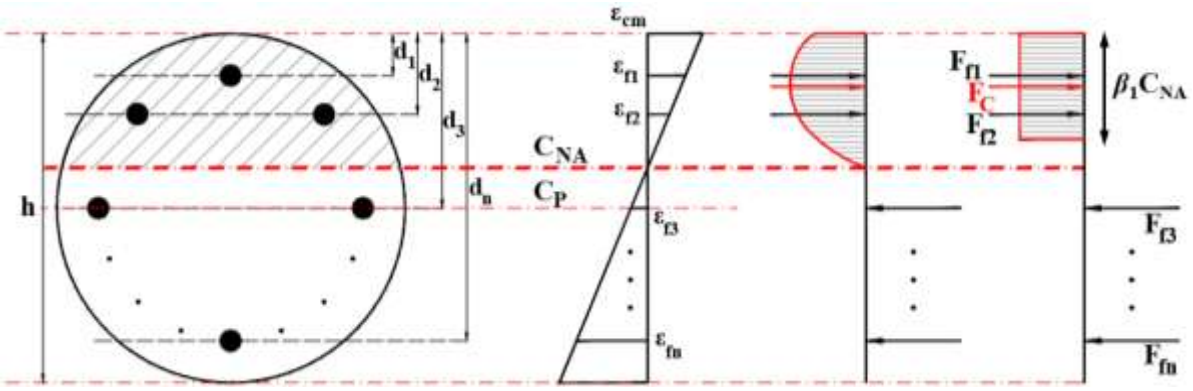

Figure 3. Parameters and assumptions for cross-sectional analysis of rectangular and circular column sections

The forces and moments at each layer of GFRP reinforcement are calculated using the strains, elastic modulus and the area of the reinforcement as described for rectangular cross sections. However, the force in the concrete is calculated as (clause 22.2.2.4):

$$F_c = 0.85 f_c' A_c \tag{11}$$

Where A_c is the area of the concrete section that the stress block is applied on (Figure 4), and is calculated as:

$$A_c = \left(\frac{\alpha}{\pi}\right) \times \left(\frac{\pi h^2}{4}\right) - x\left(\frac{h}{2} - \beta_1 C_{NA}\right) \tag{12}$$

wherein,

$$x = \left[\left(\frac{h}{2}\right)^2 + \left(\frac{h}{2} - \beta_1 C_{NA}\right)^2\right]^{0.5} \tag{13}$$

And consequently, moments around neutral axis and the center of plastic can be found by the following equations, respectively:

$$M_c = F_c[y_s - (h/2 - C_{NA})] \tag{14}$$

$$M_c' = F_c y_s \tag{15}$$

wherein, y_s is the distance of the center of hatched area in Figure 4 from the center of plastic:

$$y_s = \frac{h(\sin\alpha)^3}{3(\alpha - \sin\alpha\cos\alpha)} \tag{16}$$

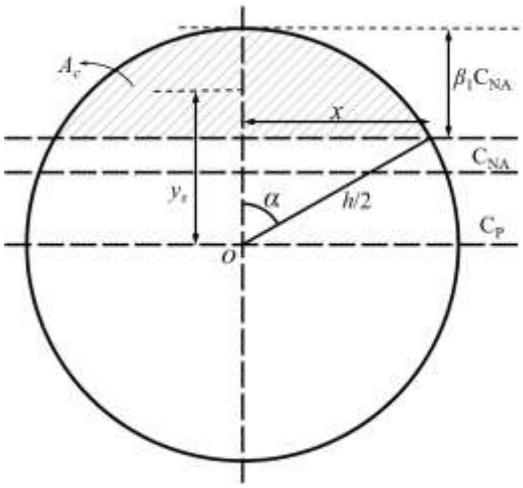

Figure 4. Definition of parameters for calculating the stress block on circular sections

The sum of concrete and GFRP bar forces gives the overall force, P_T, and moment, M_T, of the cross section for a certain location of the neutral axis, and therefore, load eccentricity can be calculated as described before. For circular columns the maximum nominal axial strength in compression, P_n, is calculated using $0.85P_0$ for columns with spirals according to clause 22.4.2 (36) based on the work by Hadhood et al. (63) on circular columns reinforced with GFRP bars and spirals. Where, P_0 is (clause 22.4.2.2):

$$P_0 = 0.85f_c'(\pi\, h^2/4) \tag{17}$$

4. INTERACTION DIAGRAMS

4.1. Model Verification

Before preparing the interaction diagrams, the results of the model are checked with an analytical benchmark model (28) in the literature for both rectangular and circular cross section columns. The concrete strength, f'_c, is 28 MPa (4 ksi) and the elastic modulus and strength of the bars are 40 GPa (6000 ksi) and 400 MPa (60 ksi), respectively. The value of strength in the benchmark study was selected equal to the strength of steel bars for comparison purposes. The square column has a 600×600 mm (24''×24'') cross section, having four layers of bars (12-ϕ25 total). The diameter of the circular column is 600 mm (24'') and it has 12-ϕ25 bars. Using the prepared model, the interaction diagrams of the square and circular columns are as presented in Figure 5 against the benchmark interaction diagram.

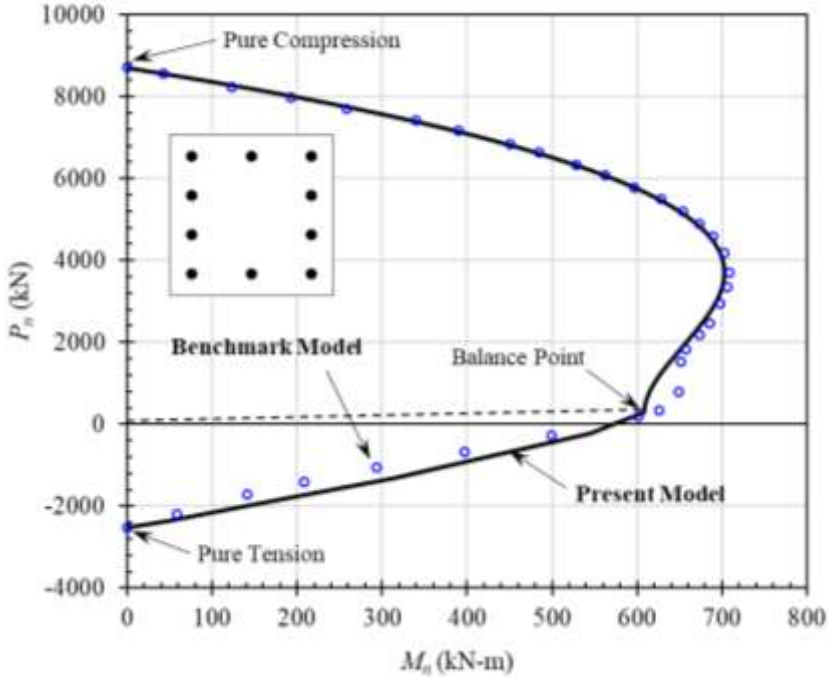

(a)

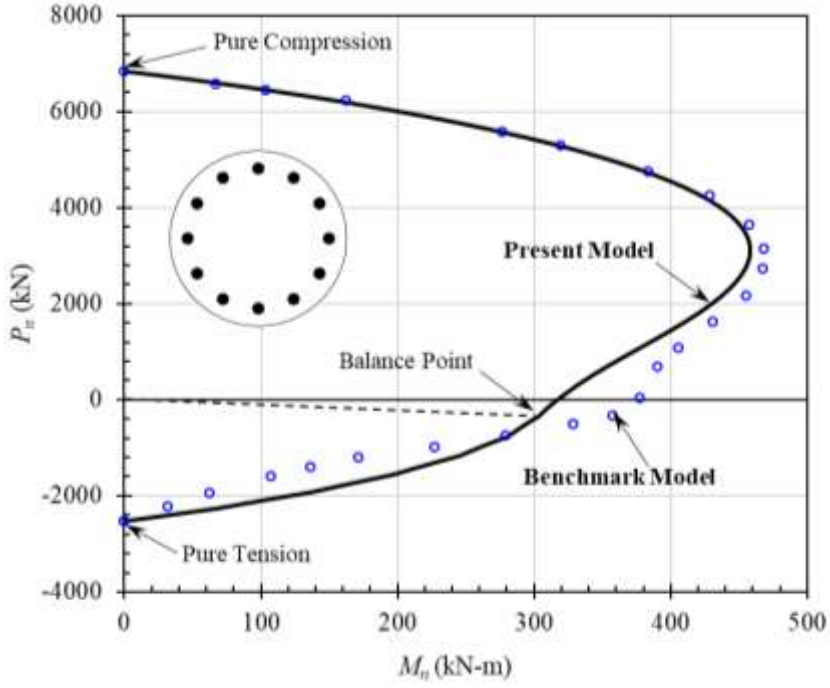

(b)

Figure 5. Interaction diagrams for a) rectangular and b) circular columns for verification of the analytical model (28)

As seen in Figure 5, there is a good agreement between the results. Minor differences originate from assumptions such as the strength reduction factor, ϕ, which was a constant in the benchmark

study per ACI 440.1R-06 (64), whereas in the present model it varies with the failure mode as defined in ACI CODE-440.11-22 (36).

In the second stage, validation was conducted using experimental results from literature. Guérin et al. (22) tested GFRP-RC columns (400×400 mm) under axial-flexural loads with four eccentricities (e/h = 0.1 to 0.8), reinforced with six #6 GFRP bars (ρ = 1%) and 40 mm cover. The compressive strength of concrete was 40 MPa, and the GFRP bars had a strength of 1317 MPa and elastic modulus of 51.3 GPa. For circular columns, Hadhood et al. (3) reported tests on 305 mm diameter columns with 8 #5 GFRP bars (ρ = 2%). The concrete strength averaged 70.2 MPa, and the bars had a strength of 1289 MPa and elastic modulus of 54.9 GPa.

Both studies included columns with slenderness ratios of 17.3 and 19.7, which are near the slenderness limit of 17 for unbraced columns per ACI CODE-440.11-22 (Clause 6.2.5). However, second-order effects were not explicitly accounted for in the original tests and are considered negligible for these cases. As such, the present model focuses on section-level analysis assuming negligible second-order effects, which is consistent with the referenced tests. The results, compared in Figure 6, show good agreement between the predicted nominal capacities and the experimental values. A more conservative diagram can be generated by applying the strength reduction factor per Clause 21.2.1 of ACI CODE-440.11-22 (36).

Moreover, the confinement effect from transverse reinforcement is not included in the model, as it is known from literature (12,18,30,45) that confinement tends to activate post-peak, contributing to residual capacity rather than initial strength.

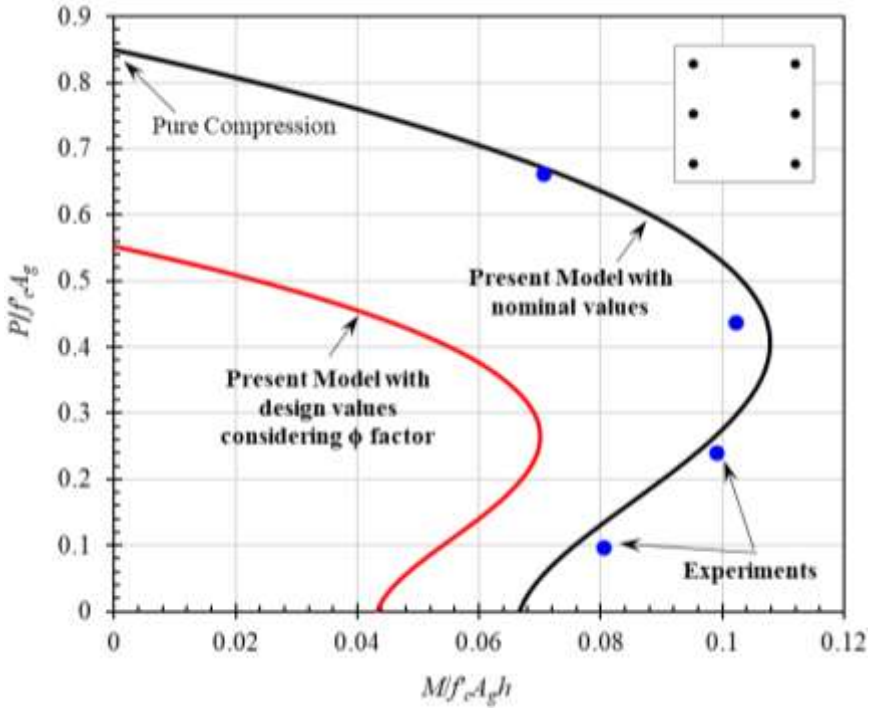

(a)

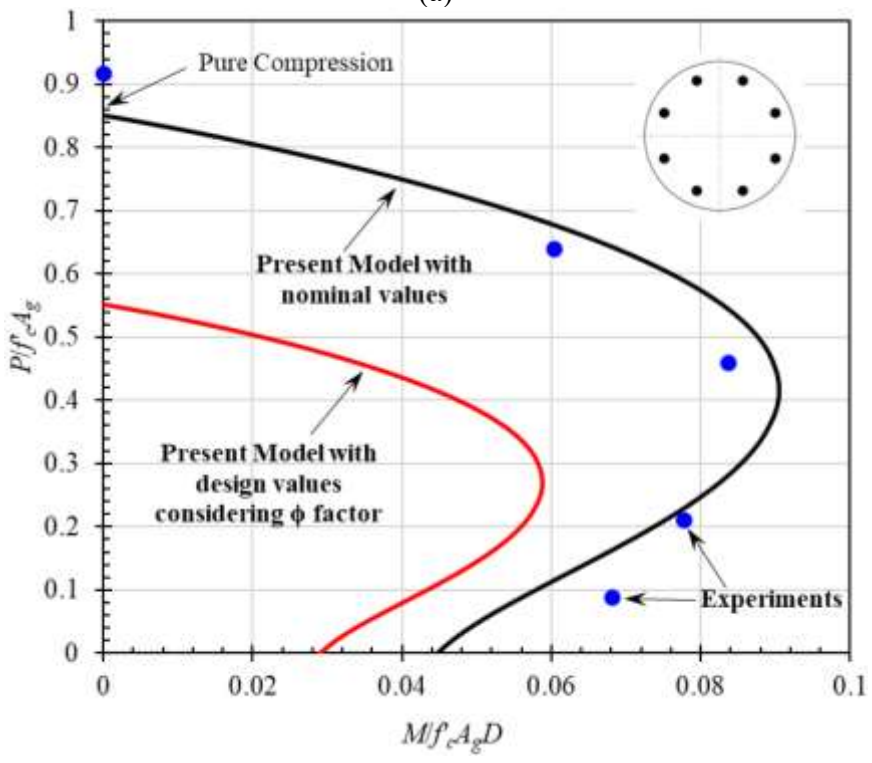

(b)

Figure 6. Comparing the interaction diagrams of the present model with the experimental data from a) Guérin et al. (22) and b) Hadhood et al. (3)

4.2. Interaction Diagrams for Design Applications

Having been verified, the model is used to produce interaction diagrams for practical ranges of material and cross-sectional properties as presented in Table 2.

Table 2. The range of parameters used in the preparation of the interaction diagrams

Parameter	Description	Range	Unit
γ	Ratio of the distance between the outer layers of reinforcement in a column to the overall depth of the column	0.6 – 0.9	–
ρ_f	Ratio of GFRP bars area to total section area	0.01 – 0.05*	–
f'_c	Compressive strength of concrete	27 – 45	MPa
E_f	Elastic modulus of GFRP reinforcement	50	GPa
f_{fu}	Design tensile strength of GFRP longitudinal reinforcement	900	MPa

* Clause 10.6.1 (36)

A standard approach is used to define the axis values, where the axial forces shown on the vertical axis are divided by the gross column cross-sectional area and then normalized by the compressive strength of concrete. Similarly, for the horizontal axis, the moment values are divided by the gross column cross-sectional area and the section height/diameter, and then normalized by f'_c. Due to the relatively large number of design figures, they are presented in Appendix A and B (Figures A1-A3 and B1-B3) for rectangular and circular columns, respectively.

Based on Figure 1, which shows the variation of the strength reduction factor, ϕ, as a function of bar strain, a compressive-controlled condition results in a factor of 0.65. In practice, the ultimate strain of bars, which can reach up to 2 percent, is rarely reached in ordinary columns subjected to eccentric compressive loads. As a result, all diagrams in the compressive domain exhibit a strength reduction factor of 0.65. Taking this into account, and neglecting the compressive strength of the bars, the design axial strength from clause 22.4.2.2 (36) is used with reduction factors of 0.8 and 0.85 for rectangular columns with ties and circular columns with spirals, respectively, as per clause 22.4.2.1 (36), to calculate $P_{n,max}$.

The code imposes design restrictions on the strains (clause 10.3.2) and, if the factored axial compression, P_u, determined from the analysis of the loads on the column, exceeds $0.1f'_cA_g$, the

ultimate tensile strain of the bars is limited to 1 percent to prevent excessive deformations. While this constraint is incorporated in the analytical model, the strains are typically below 1 percent in the practical range of concrete and GFRP bar material properties under eccentric compressive loads.

Although the most practical values were selected as the material properties of GFRP reinforcement, considering a range of available elastic modulus and ultimate tensile strength values can further generalize the interaction diagrams. However, this approach was not taken in this study to avoid any confusion in using diagrams.

5. PARAMETRIC STUDIES

5.1. Concrete Behavior Modeling

A comparative study was conducted to examine the effect of using the actual stress block in the cross-sectional analysis of columns, as opposed to the equivalent rectangular stress block. The stress-strain behavior of concrete in compression was modeled using two well-known constitutive models proposed by Popovics (50) and Thorenfeldt (51). The Popovics model was defined by the following relationship:

$$f_c = f_c' \frac{\varepsilon_c}{\varepsilon_c'} \frac{n}{n - 1 + \left(\frac{\varepsilon_c}{\varepsilon_c'}\right)^n} \tag{18}$$

Wherein, f_c' is the concrete ultimate strength and n is the curve fitting number defined as:

$$n = \frac{E_c}{\left(E_c - \frac{f_c'}{\varepsilon_c'}\right)} \tag{19}$$

ε_c' is the strain of concrete corresponding to its ultimate strength:

$$\varepsilon_c' = 1.7 \frac{f_c'}{E_c} \tag{20}$$

The model presented by Thorenfeldt (51) has a similar format but incorporates a stress decay factor, *k*, to the equation:

$$f_c = f_c' \frac{\varepsilon_c}{\varepsilon_c'} \frac{n}{n - 1 + \left(\frac{\varepsilon_c}{\varepsilon_c'}\right)^{nk}} \tag{21}$$

And

$$k = 0.67 + \frac{f_c'}{62} \ (MPa) \tag{22}$$

In both equations, the elastic modulus of concrete, E_c, is defined as:

$$E_c = 4700\sqrt{f_c'} \ (MPa) \tag{23}$$

$$E_c = 3320\sqrt{f_c'} + 6900 \ (MPa) \tag{24}$$

Eq. (23) is used for normalweight concrete (52), with f'_c up to 40 MPa, while Eq. (24) is used for high-strength concrte (65), with f'_c up to 83 MPa. The same procedure used for the equivalent stress block method was applied, with the only difference being that the concrete at the top of the neutral axis (on the compression side) was divided into layers, each with a height of 0.001 inches. The corresponding forces and moments were then calculated for the concrete. To compare the results, interaction diagrams are presented for three different approaches, where γ=0.75, f'_c=35 MPa, and the other parameters are consistent with those in Table 2. As shown in Figure 7, the equivalent stress block method is a relatively more conservative approach for design purposes. The difference between the diagrams for both rectangular and circular cross-sections is approximately 10%. This suggests that a scaling factor of 1.1 can be applied to the code calculations to adjust them according to the actual stress-strain block.

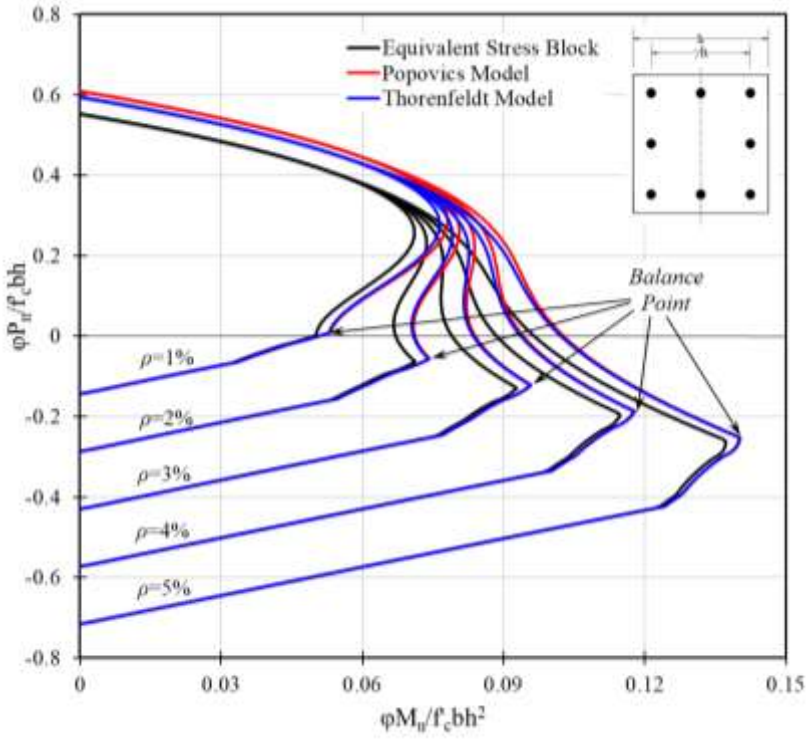

(a)

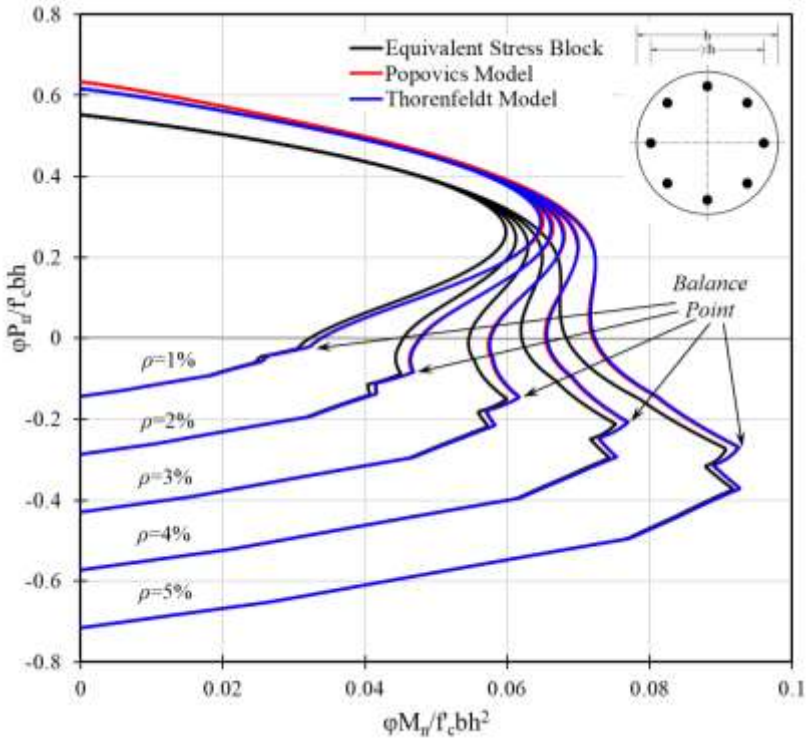

(b)

Figure 7. Comparing the interaction diagrams from the three approaches for concrete stress modeling: a) Rectangular and b) Circular cross-section columns

Negative axial forces indicate conditions where the column is under tensile loading. The tensile portion of the interaction diagram intersects the vertical axis at the maximum relative tensile strength of the bars. Below the balance point, the tensile portion depends on the behavior of the bars and is, therefore, unaffected by the concrete stress modeling approach. In the traditional method for determining the interaction diagram of steel-reinforced concrete columns, the balance point is typically located around the maximum moment location of the diagram. However, for GFRP-RC columns, the balance point's location depends on several factors, including the material properties and ratio of GFRP reinforcement, column dimensions, the γ factor, and the compressive strength of the concrete (66). Most often, this point lies on the tension side of the interaction diagram. However, as shown in Appendix A, for small amounts of reinforcement, this point may shift to the compression side of the diagram. The balance point serves as a critical indicator in design, as it helps distinguish between compression- and tension-controlled failure modes, guiding reinforcement selection and section optimization for GFRP-RC columns.

The shape of the interaction diagram for GFRP-RC columns is influenced by the ratio of concrete compressive strength to bar tensile strength, the ratio of the concrete elastic modulus to the GFRP elastic modulus, and the reinforcement ratio. As shown in Figure 7, increasing the reinforcement ratio while keeping other contributing factors constant causes the intersection point of the diagram with the horizontal axis to shift toward higher moments, while also moving the balance point toward larger tensile axial loads. Further analysis of the effects of the reinforcement bars is provided in the following section.

5.2. GFRP Reinforcement Material Properties

To investigate the effect of reinforcement material properties, three different ratios of bar ultimate tensile strength to concrete strength, f_{ftu}/f'_c, (Figure 8), and three different ratios of elastic modulus,

E_f/E_c, (Figure 9), were considered for both rectangular and circular cross section columns. In all diagrams the compressive strength of concrete is 35 MPa, the reinforcement ratio is at an average value of 3 percent, and γ is 0.75. Three different values were assumed for the ultimate tensile strength of the bars (700, 900, and 1100 MPa), and three different values were considered for the elastic modulus (40, 50, and 60 GPa).

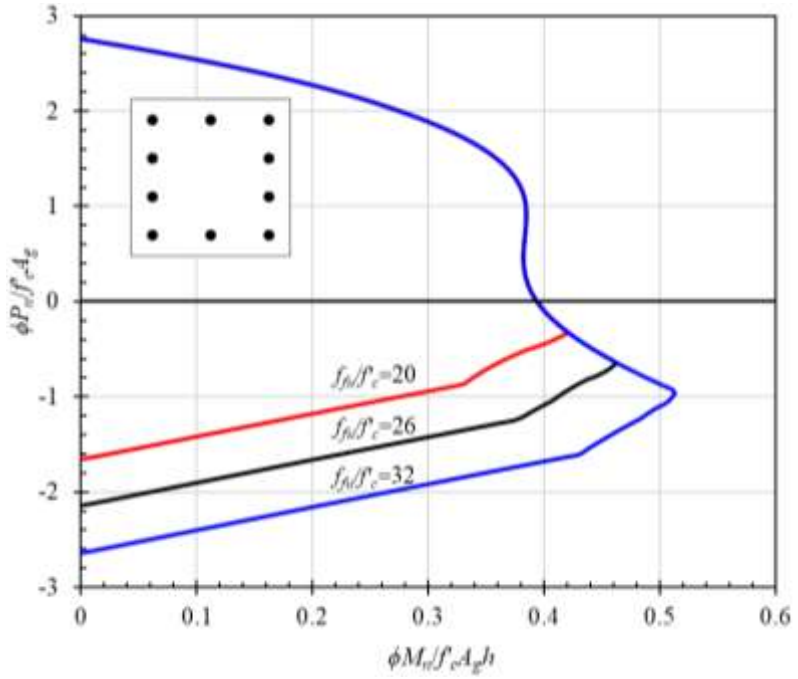

(a)

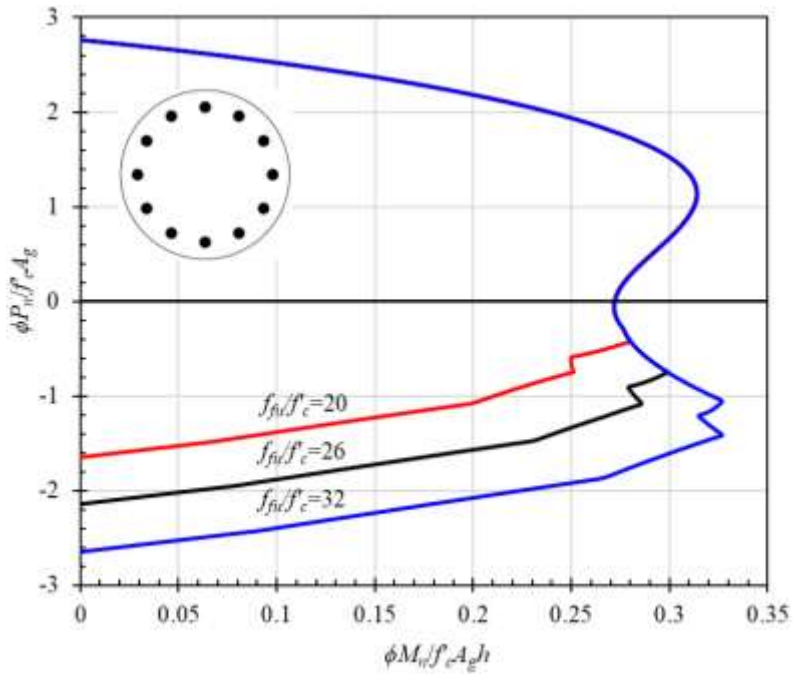

(b)

Figure 8. Studying the ratio of the tensile strength of reinforcement to compressive strength of concrete for a) rectangular and b) circular columns

As can be seen in Figure 8, since the compressive strength of bars is neglected, the strength ratio had no effect on the compression side of the interaction diagrams for both rectangular and circular cross sections. However, the position of the balance point, which directly depends on the tensile strength of the bars, shifted with change in the ratio of f_{ftu}/f'_c. The higher the f_{ftu}, the more moment resistance is observed. Meanwhile, it can be seen in the tension side that the higher the ratio, the greater area that the diagram covers and the maximum tensile strength of the column increased.

Looking at Figure 9, the elastic modulus of the reinforcement affected the compression side of the diagram up to the point that from there to the pure compression point, all the bars are under compression and therefore they have no contribution in the diagram. It is seen that lower elastic modulus of the rebras means more contribution of concrete. According to this figure, rebras elastic modulus affect the diagram in a specific zone, which is from the balance point in the tensile part up to the point that all the bars are under compression and neglected.

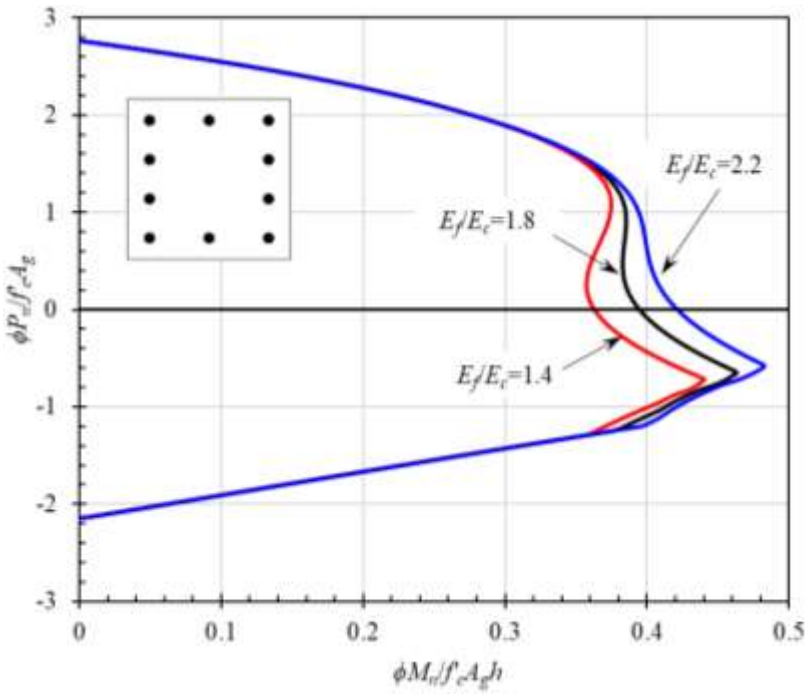

(a)

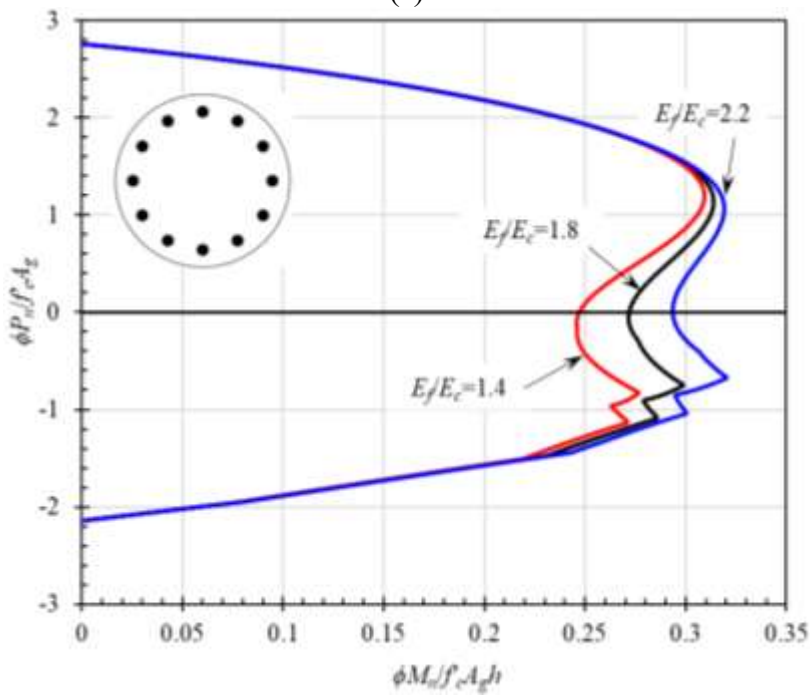

(b)

Figure 9. Studying the ratio of the elastic modulus of reinforcement to concrete for a) rectangular and b) circular columns

The practical interaction diagrams provided in the Appendices are based on average values of elastic modulus (50 GPa) and tensile strength (900 MPa). Designers can adjust the interaction diagrams using the trends demonstrated in Figures 8 and 9. Specifically, the interaction diagram

values can be scaled or modified according to the actual tensile strength and elastic modulus of the bars used in practice.

6. CONCLUSION

This paper presents interaction diagrams as a simple and practical design tool for practicing engineers to design rectangular and circular concrete columns reinforced with GFRP bars, in accordance with the requirements of ACI CODE-440.11-22 (36). The analytical model used in this study employs cross-sectional analysis to determine the stresses and strains in the FRP bars and concrete under various combinations of axial compressive loads and corresponding moments caused by load eccentricity. The following findings were obtained from this study:

- The ACI CODE-440.11-22 stress distribution approach was compared with the Popovics and Thorenfeldt models. It was found that the equivalent stress block method is more conservative, with a 10% difference between the diagrams for rectangular and circular cross-sections. A scaling factor of 1.1 can be applied to adjust the code calculations for the actual stress-strain block. Future reliability analysis is recommended to optimize this factor.
- The location of the balance point in the interaction diagram for GFRP-RC columns depends on factors such as material properties, reinforcement ratio, column dimensions, and concrete compressive strength. Unlike steel-RC columns, this point is typically on the tension side of the diagram. For low reinforcement ratios (e.g., 1%), it may shift to the positive axial load side. Increasing the reinforcement ratio while keeping other factors constant shifts the intersection point of the diagram with the horizontal axis toward higher moments and moves the balance point toward larger tensile loads.
- The design axial strength in clause 22.4.2.2 of ACI CODE-440.11-22 is a limiting condition, and the compressive-controlled condition results in a strength reduction factor

of 0.65 for all diagrams in the compressive domain. Reduction factors of 0.8 and 0.85 are considered for rectangular columns with ties and circular columns with spirals, respectively.

- The ultimate tensile strain of the bars is limited to 1 percent to prevent excessive deformations in clause 10.3.2 of ACI CODE-440.11-22. However, this constraint is typically not a concern in practical situations under eccentric compressive loads, as the strains in bars are usually below 1 percent.
- Since the compressive strength of bars is neglected in the code approach, the strength ratio of the bars does not affect the compression side of the interaction diagram but significantly influences the tension side. Additionally, the elastic modulus of reinforcement plays a critical role in the tension side; as the elastic modulus increases, the interaction diagram's area decreases, indicating that higher strength and stiffness of the reinforcement improve its efficiency in resisting tension.

REFERENCES

1. Afifi MZ, Mohamed HM, Benmokrane B. Axial capacity of circular concrete columns reinforced with GFRP bars and spirals. Journal of Composites for Construction. 2014;18(1):04013017.
2. De Luca A, Matta F, Nanni A. Behavior of full-scale glass fiber-reinforced polymer reinforced concrete columns under axial load. ACI Struct J. 2010;107(5):589.
3. Hadhood A, Mohamed HM, Benmokrane B. Experimental study of circular high-strength concrete columns reinforced with GFRP bars and spirals under concentric and eccentric loading. Journal of Composites for Construction. 2017;21(2):04016078.
4. Hadhood A, Mohamed HM, Ghrib F, Benmokrane B. Efficiency of glass fiber-reinforced polymer (GFRP) discrete hoops and bars in concrete columns under combined axial and flexural loads. Compos B Eng. 2017;114:223–36.
5. Hadi MNS, Hasan HA, Sheikh MN. Experimental investigation of circular high-strength concrete columns reinforced with glass fiber-reinforced polymer bars and helices under different loading conditions. Journal of Composites for Construction. 2017;21(4):04017005.
6. Hadi MNS, Karim H, Sheikh MN. Experimental investigations on circular concrete columns reinforced with GFRP bars and helices under different loading conditions. Journal of Composites for Construction. 2016;20(4):04016009.

7. Khorramian K, Sadeghian P. Experimental and analytical behavior of short concrete columns reinforced with GFRP bars under eccentric loading. Eng Struct. 2017;151:761–73.

8. Maranan GB, Manalo AC, Benmokrane B, Karunasena W, Mendis P. Behavior of concentrically loaded geopolymer-concrete circular columns reinforced longitudinally and transversely with GFRP bars. Eng Struct. 2016;117:422–36.

9. Elchalakani M, Ma G. Tests of glass fibre reinforced polymer rectangular concrete columns subjected to concentric and eccentric axial loading. Eng Struct. 2017;151:93–104.

10. Elchalakani M, Karrech A, Dong M, Ali MSM, Yang B. Experiments and finite element analysis of GFRP reinforced geopolymer concrete rectangular columns subjected to concentric and eccentric axial loading. Structures. 2018;14:273–89.

11. Mohamed HM, Afifi MZ, Benmokrane B. Performance evaluation of concrete columns reinforced longitudinally with FRP bars and confined with FRP hoops and spirals under axial load. Journal of Bridge Engineering. 2014;19(7):04014020.

12. Tobbi H, Farghaly AS, Benmokrane B. Concrete Columns Reinforced Longitudinally and Transversally with Glass Fiber-Reinforced Polymer Bars. ACI Struct J. 2012;109(4).

13. Tobbi H, Farghaly AS, Benmokrane B. Behavior of Concentrically Loaded Fiber-Reinforced Polymer Reinforced Concrete Columns with Varying Reinforcement Types and Ratios. ACI Struct J. 2014;111(2).

14. Tobbi H, Farghaly AS, Benmokrane B. Strength model for concrete columns reinforced with fiber-reinforced polymer bars and ties. ACI Struct J. 2014;111(4):789–98.

15. Barua S, El-Salakawy E. Performance of GFRP-reinforced concrete circular short columns under concentric, eccentric, and flexural loads. Journal of Composites for Construction. 2020;24(5):04020044.

16. Elmesalami N, Abed F, Refai A El. Concrete columns reinforced with GFRP and BFRP bars under concentric and eccentric loads: Experimental testing and analytical investigation. Journal of Composites for Construction. 2021;25(2):04021003.

17. Tahir M, Karam MS, Hassam M, Umer M, Hameed R. Numerical evaluation of axial compressive behavior of hollow concrete columns reinforced with GFRP bars and spirals. Structural Concrete. 2024;25(1):566–82.

18. Hadi MNS, Youssef J. Experimental investigation of GFRP-reinforced and GFRP-encased square concrete specimens under axial and eccentric load, and four-point bending test. Journal of Composites for Construction. 2016;20(5):04016020.

19. Youssef J, Hadi MNS. Axial load-bending moment diagrams of GFRP reinforced columns and GFRP encased square columns. Constr Build Mater. 2017;135:550–64.

20. Hadhood A, Mohamed HM, Benmokrane B. Axial load–moment interaction diagram of circular concrete columns reinforced with CFRP bars and spirals: Experimental and theoretical investigations. Journal of Composites for Construction. 2017;21(2):04016092.

21. Sun L, Wei M, Zhang N. Experimental study on the behavior of GFRP reinforced concrete columns under eccentric axial load. Constr Build Mater. 2017;152:214–25.

22. Guérin M, Mohamed HM, Benmokrane B, Shield CK, Nanni A. Effect of Glass Fiber-Reinforced Polymer Reinforcement Ratio on Axial-Flexural Strength of Reinforced Concrete Columns. ACI Struct J. 2018;115(4).

23. Raza A, El Ouni MH, uz Zaman Khan Q, Berradia M. Structural assessment of eccentrically loaded GFRP reinforced circular concrete columns: Experiments and finite element analysis. Compos Struct. 2021;275:114528.

24. Elchalakani M, Dong M, Karrech A, Mohamed Ali MS, Huo JS. Circular concrete columns and beams reinforced with GFRP bars and spirals under axial, eccentric, and flexural loading. Journal of Composites for Construction. 2020;24(3):04020008.

25. Khorramian K, Sadeghian P. Experimental investigation of short and slender rectangular concrete columns reinforced with GFRP bars under eccentric axial loads. Journal of Composites for Construction. 2020;24(6):04020072.

26. Karimi Pour A, Shirkhani A, Kırgız MS, Noroozinejad Farsangi E. Experimental investigation of GFRP-reinforced concrete columns made with waste aggregates under concentric and eccentric loads. Structural Concrete. 2023;24(1):1670–88.

27. Al-Thairy H. Behavior and design of eccentrically compressed hybrid steel and GFRP reinforced concrete columns at elevated temperature. Structural Concrete. 2024;

28. Jawaheri Zadeh H, Nanni A. Design of RC columns using glass FRP reinforcement. Journal of Composites for Construction. 2013;17(3):294–304.

29. Afifi MZ, Mohamed HM, Benmokrane B. Strength and axial behavior of circular concrete columns reinforced with CFRP bars and spirals. Journal of Composites for Construction. 2014;18(2):04013035.

30. Afifi MZ, Mohamed HM, Chaallal O, Benmokrane B. Confinement model for concrete columns internally confined with carbon FRP spirals and hoops. Journal of Structural Engineering. 2015;141(9):04014219.

31. Guérin M, Mohamed HM, Benmokrane B, Nanni A, Shield CK. Eccentric Behavior of Full-Scale Reinforced Concrete Columns with Glass Fiber-Reinforced Polymer Bars and Ties. ACI Struct J. 2018;115(2).

32. Karim H, Noel-Gough B, Sheikh MN, Hadi MNS. Strength and ductility behavior of circular concrete columns reinforced with GFRP bars and helices. In: The 12th International Symposium on Fiber Reinforced Polymers for Reinforced Concrete Structures (FRPRCS-12). 2015.

33. Pantelides CP, Gibbons ME, Reaveley LD. Axial load behavior of concrete columns confined with GFRP spirals. Journal of Composites for Construction. 2013;17(3):305–13.

34. Ali MA, El-Salakawy E. Seismic performance of GFRP-reinforced concrete rectangular columns. Journal of Composites for Construction. 2016;20(3):04015074.

35. Tavassoli A, Sheikh SA. Seismic resistance of circular columns reinforced with steel and GFRP. Journal of Composites for Construction. 2017;21(4):04017002.

36. ACI. ACI CODE-440.11-22: Building Code Requirements for Structural Concrete Reinforced with Glass Fiber-Reinforced Polymer (GFRP) Bars-Code and Commentary. American Concrete Institute; 2022.

37. ACI. ACI PRC-440.1R-15: Guide for the Design and Construction of Structural Concrete Reinforced with FRP Bars. Farmington Hills, MI: American Concrete Institute; 2015.

38. CSA. S6:19 - Canadian Highway Bridge Design Code. Canadian Standards Association; 2019.

39. Jawaheri Zadeh H, Nanni A. Flexural stiffness and second-order effects in fiber-reinforced polymer-reinforced concrete frames. ACI Struct J. 2017;114(2):533.

40. Abdelazim W, Mohamed HM, Afifi MZ, Benmokrane B. Proposed slenderness limit for glass fiber-reinforced polymer-reinforced concrete columns based on experiments and buckling analysis. ACI Struct J. 2020;117(1):241–54.

41. Mirmiran A, Yuan W, Chen X. Design for slenderness in concrete columns internally reinforced with fiber-reinforced polymer bars. Structural Journal. 2001;98(1):116–25.

42. Syed AU, Goldack A. Slenderness limit for GFRP reinforced concrete columns based on axial force ratio. Eng Struct. 2024;298:117026.

43. Salah-Eldin A, Mohamed HM, Benmokrane B. Structural performance of high-strength-concrete columns reinforced with GFRP bars and ties subjected to eccentric loads. Eng Struct. 2019;185:286–300.

44. Wang T, Li L, Dou L, Huang Q, Zhou Z, Cao Y, et al. Behavior of GFRP reinforced concrete columns confined with inner steel spirals. Structural Concrete. 2025;26(1):779–93.

45. Sadat Hosseini A, Sadeghian P. Transverse Reinforcement Configurations in GFRP-Reinforced Concrete Columns: Experiments and Damage Mechanics-Based Modeling. Journal of Building Engineering. 2025;112368.

46. Nouri Y, Ghanizadeh AR, Safi Jahanshahi F, Fakharian P. Data-driven prediction of axial compression capacity of GFRP-reinforced concrete column using soft computing methods. Journal of Building Engineering. 2025;101:111831.

47. Selmy YM, Abdallah AE, El-Salakawy Ehab F. Seismic Performance Assessment of GFRP-RC Circular Columns under High Torsion Combined with Bending and Shear Cyclic Loading. Journal of Composites for Construction. 2025 Feb 1;29(1):04024080.

48. Lin G, Zeng JJ, Liang SD, Liao J, Zhuge Y. Seismic behavior of novel GFRP bar reinforced concrete beam-column joints internally reinforced with an FRP tube. Eng Struct. 2022;273:115100.

49. Lin G, Zhang SS. Contribution of longitudinal GFRP bars in concrete filled FRP tubular (CFFT) cylinders under monotonic or cyclic axial compression. Eng Struct. 2023;281:115766.

50. Popovics S. A numerical approach to the complete stress-strain curve of concrete. Cem Concr Res. 1973;3(5):583–99.

51. Thorenfeldt E. Mechanical properties of high-strength concrete and applications in design. In: Symposium Proceedings, Utilization of High-Strength Concrete, Norway, 1987. 1987.

52. ACI. ACI 318-19: Building Code Requirements for Structural Concrete and Commentary. American Concrete Institute; 2019.

53. Hadhood A, Mohamed HM, Ghrib F, Benmokrane B. Efficiency of glass-fiber reinforced-polymer (GFRP) discrete hoops and bars in concrete columns under combined axial and flexural loads. Compos B Eng. 2017;114:223–36.

54. Tahir M, Wang Z, Wei Z, Jameel R. Numerical and analytical modeling of FRP-reinforced concrete columns subjected to compression loading. Australian Journal of Structural Engineering. 2021;22(2):96–109.

55. Sadat Hosseini A, Sadeghian P. Effects of square spiral pitch and tie overlap on the behavior of GFRP-reinforced concrete columns under concentric and eccentric loads. Structures. 2025;76:108947.

56. Sadat Hosseini A, Sadeghian P. Slenderness effect on GFRP-RC columns with square spirals under concentric and eccentric loading: Experimental and analytical study. Eng Struct. 2025;334:120277.

57. ASTM. ASTM D7205/D7205M, Standard Test Method for Tensile Properties of Fiber-Reinforced Polymer Matrix Composite Bars. 2021.

58. AlAjarmeh OS, Manalo AC, Benmokrane B, Vijay P V, Ferdous W, Mendis P. Novel testing and characterization of GFRP bars in compression. Constr Build Mater. 2019;225:1112–26.

59. Khorramian K, Sadeghian P. Material characterization of GFRP bars in compression using a new test method. J Test Eval. 2021;49(2):1037–52.

60. D'Antino T, Pisani MA. Tensile and compressive behavior of thermoset and thermoplastic GFRP bars. Constr Build Mater. 2023;366:130104.

61. Sadat Hosseini A, Velkumar SK, Sadeghian P. Behavior of GFRP-Reinforced Concrete Members under Combined Bending Moment and Low Axial Load. Journal of Composites for Construction. 2024;28(4):04024025.

62. Sadat Hosseini A, Sadeghian P. Assessing Compressive Properties of GFRP Bars: Novel Test Fixture and Statistical Analysis. Journal of Composites for Construction. 2025;29(2):04025011.

63. Hadhood A, Mohamed HM, Benmokrane B. Flexural stiffness of GFRP-and CFRP-RC circular members under eccentric loads based on experimental and curvature analysis. ACI Struct J. 2018;115(4):1185–98.

64. ACI. ACI PRC-440.1R-06: Guide for the design and construction of structural concrete reinforced with FRP bars. American Concrete Institute; 2006.

65. ACI. ACI PRC-363-10 Report on High-Strength Concrete. American Concrete Institute; 2010.

66. Sadat Hosseini A, Sadeghian P. Interaction Diagram of Short Concrete Columns Reinforced with GFRP Rebars. In: Canadian Society of Civil Engineering Annual Conference. Springer; 2023. p. 213–23.

Appendix A. Interaction Diagrams for Rectangular Cross-Sectional Short Columns

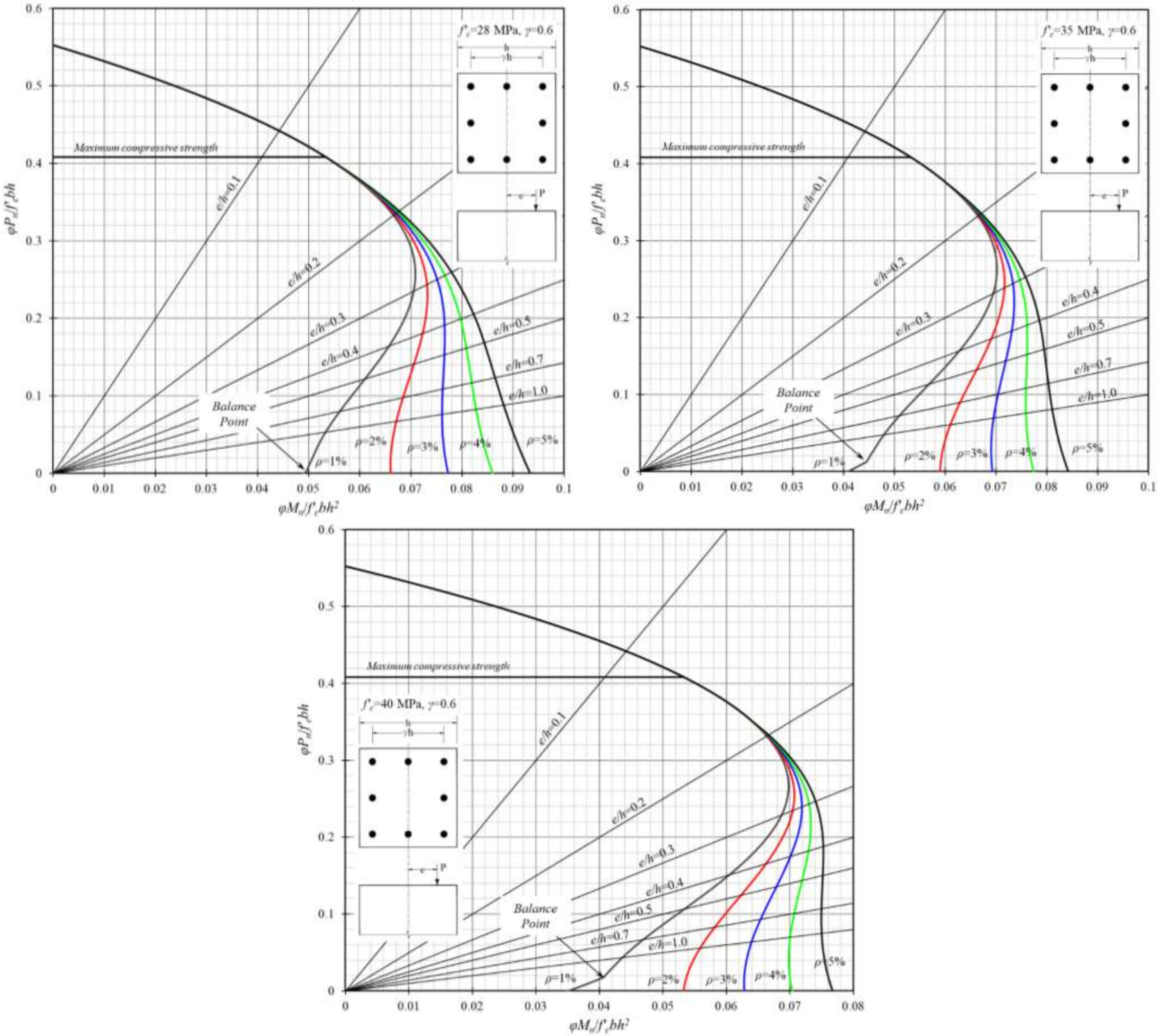

Figure A1. Interaction diagrams for rectangular sections; γ=0.6, f_{ftu}=900 MPa, and E_f=50 GPa

3

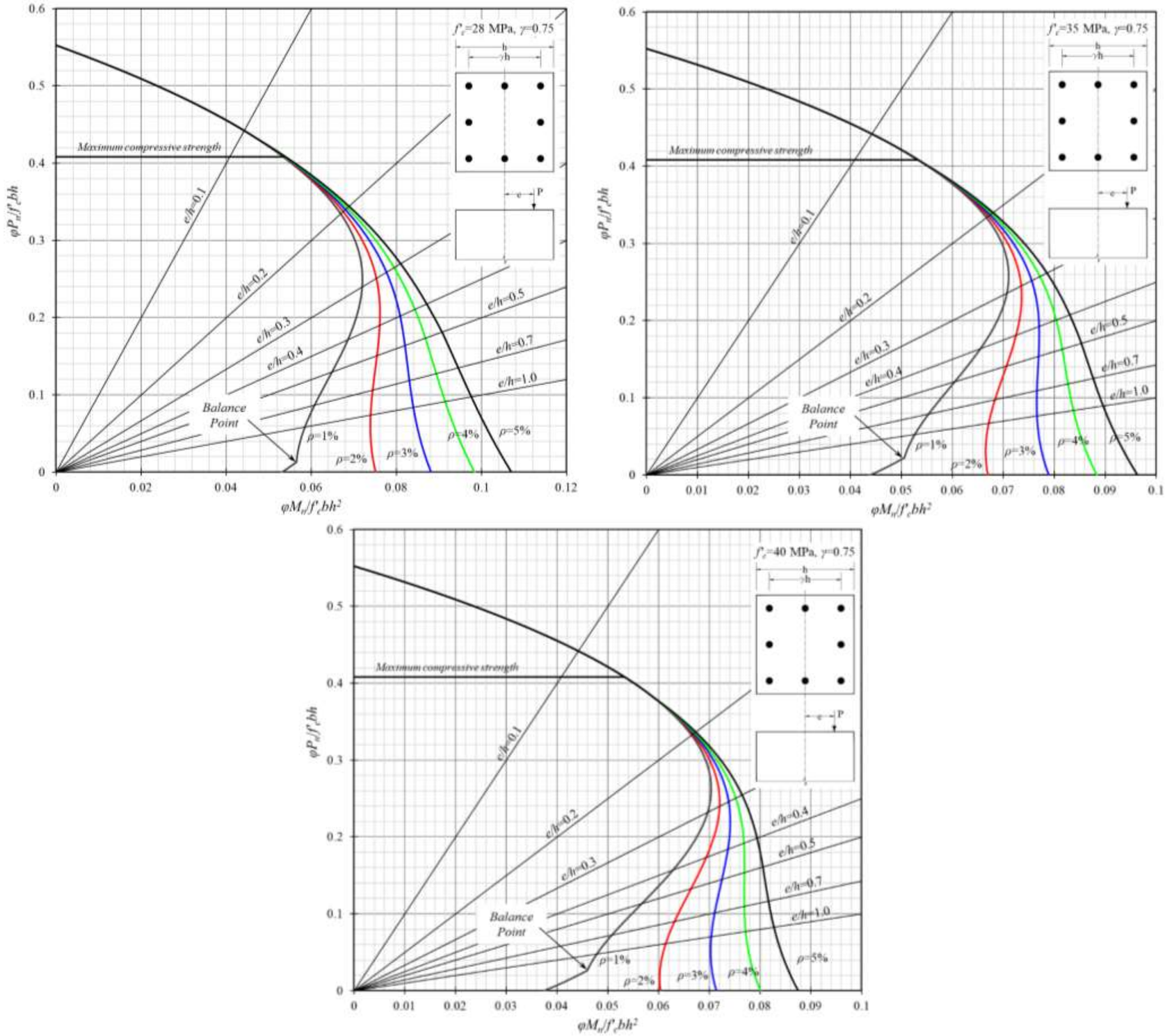

4 **Figure A2. Interaction diagrams for rectangular sections; γ=0.75, f_{ftu}=900 MPa, and E_f=50 GPa**

5

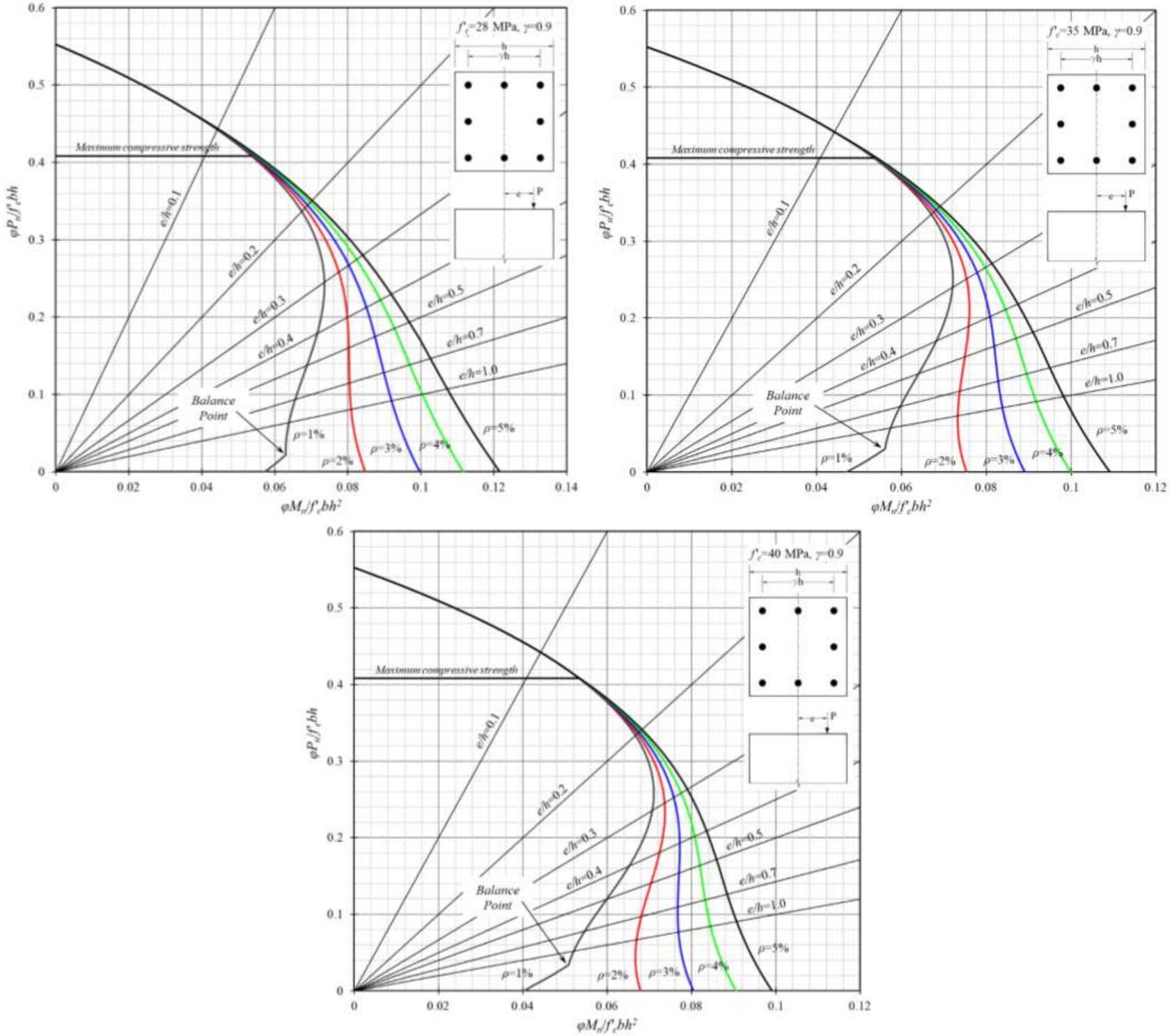

Figure A3. Interaction diagrams for rectangular sections; γ=0.9, f_{fiu}=900 MPa, and E_f=50 GPa

Appendix B. Interaction Diagrams for Circular Cross-Sectional Short Columns

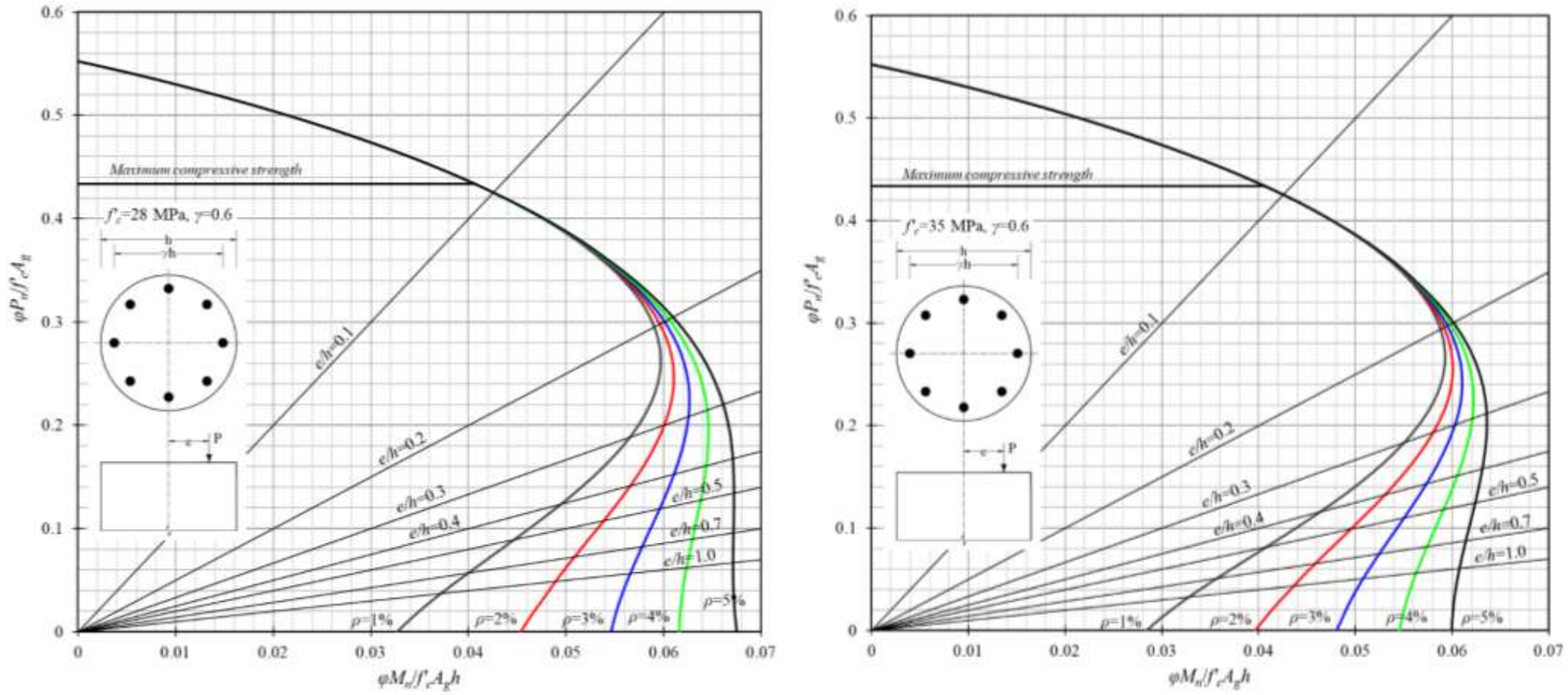

Figure B1. Interaction diagrams for circular sections; γ=0.6, f_{ftu}=900 MPa, and E_f=50 GPa

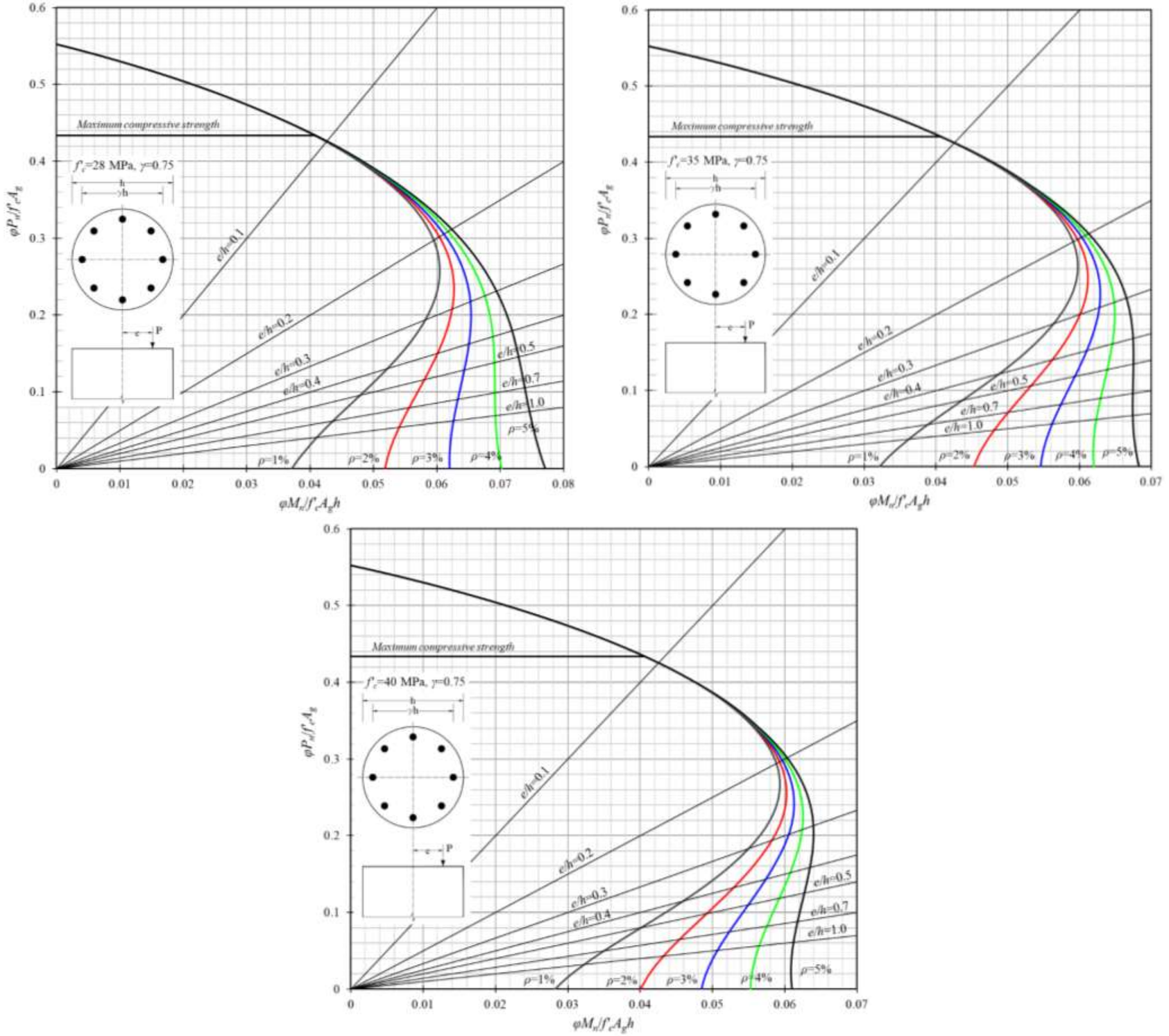

Figure B2. Interaction diagrams for circular sections; γ=0.75, f_{fu}=900 MPa, and E_f=50 GPa

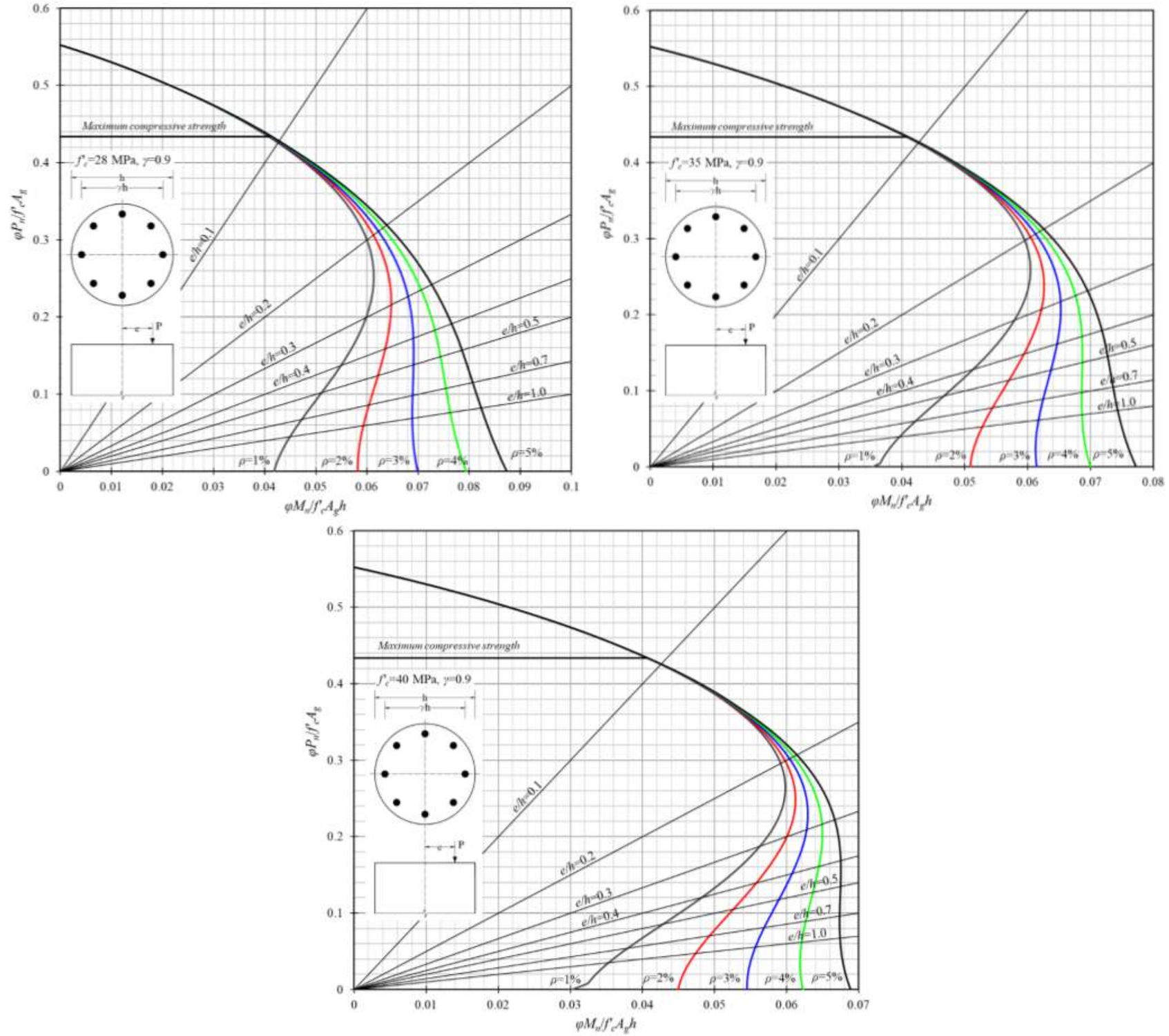

Figure B3. Interaction diagrams for circular sections; γ=0.9, f_{ftu}=900 MPa, and E_f=50 GPa